AIAA JOURNAL
Vol. 33, No. 7, July 1995

Supersonic Flux-Split Procedure for Second Moments of Turbulence

Foluso Ladeinde*
State University of New York at Stony Brook, Stony Brook, New York 11794-2300

A finite volume procedure which combines flux-difference splitting and flux-vector splitting is presented in this paper. The diffusive fluxes are treated explicitly to preserve the upwinding structure of the split Euler fluxes. This procedure is extended in this paper from its essentially laminar or eddy viscosity form to include the equations for the six components of the Reynolds stress tensor and an additional equation for the solenoidal dissipation. The models used for the unclosed terms are presented as are the extensions of the numerical procedures to cover the turbulence equations. To validate the proposed procedures, a compressible turbulent flow over a flat plate at Mach number $M_\infty = 2.87$ and Reynolds number per unit length Re/m of 6.5×10^7 was calculated and compared with experimental measurements. Also simulated was the case when the foregoing boundary-layer flow was made to pass over a ramp. A strong adverse pressure gradient case in which boundary-layer thickness-to-curvature ratio (δ/R_c) is 0.1 was considered. In this case, the supersonic turbulent boundary layer experiences the combined effects of an adverse pressure gradient, bulk compression, and concave streamline curvature. For the various tests, the results obtained from our calculations are in agreement with the experimental measurements.

I. Introduction

IT seems that the computational fluid dynamics (CFD) approach to generate engineering design data is slowly gaining the acceptance of designers of aerodynamic systems. The potential of this approach to revolutionize aircraft analysis is exemplified by impressive calculations such as those of vortex asymmetry in a high-angle-of-attack flow about a body in supersonic and subsonic flow[1] and the complex flows over ogive-cylinder impinging shock-expansion flows.[2] Unfortunately, many aerodynamic systems of interest involve turbulent or transitional flows and, because of our inadequate knowledge of these phenomena, the realization of the potential of CFD is severely hampered. Moreover, for realistic systems, turbulence investigation approaches such as direct numerical simulation (DNS) are quite inappropriate, because of the high-computational cost. Also, the large eddy simulation (LES) method has not matured to a level where it can be used to generate engineering design data for realistic problems. Thus, turbulence modeling appears to be the most feasible approach to obtain design data.

Turbulence models tend to be hierarchical. Exemplifying the zero-equation types is the Baldwin and Lomax model[3]; an approach that has received a lot of attention from the aerodynamic community, but one whose applicability is limited in complex, separated flow situations. The problem with this approach is the universal near-wall length formulation. One-equation models, which are the next in the hierarchy, also have limitations that limit their applicability in complex engineering systems. Two-equation models, of which k–ϵ and k–ω are the most popular are, in principle, more general and have been used, although with limited success, in predicting three-dimensional flows, including shock-wave/boundary-layer interactions. However, two-equation methods have an inherent weakness which stems from the assumption that the Reynolds stress tensor is aligned with the mean strain tensor. With this kind of assumption one does not expect to accurately model normal stresses and, consequently, two-equation models give poor predictions of turbulence production and pressure strain when used for flows where the normal stresses are important such as nonparallel flows.[4]

Although improvements are constantly being suggested,[2] the basic problem with the two-equation approach remains unresolved. Thus, inspite of the higher cost, it seems that second-moment closures might be needed to solve many of the complicated engineering flow problems (see Lee et al.[4] and the references therein). We are also interested in second-moment calculations because they provide more data for fundamental studies, compared to the lower order closures. An example of such data is the structural parameter (defined later in this paper), which is important in studies of coherent structures in supersonic turbulent boundary layers.[5] Because the normal stresses are involved, we do not expect current two-equation models to give reasonable calculation of this quantity.[4]

Until recently, turbulence modeling efforts were concentrated on incompressible flows. But attempts to apply variable density extensions of these incompressible models to compressible flows have not been successful,[6] implying the need for explicit compressibility terms in the models. The failure of two-equation models in predicting the von Karman constant κ in compressible flows has been discussed,[7] and an expression for the dependence of κ on turbulent Mach number M_t has been suggested.[7] Also, it is now believed that, in second-moment closures, pressure dilatation $\overline{pu_{j,j}} \equiv \overline{p\theta}$ terms (θ is fluctuating dilatation) must be added explicitly, for any chance to simulate realistic high-speed aerodynamic systems.[8–11] Further, for zero pressure gradient turbulent boundary layer (TBL), and perhaps for some other flows, the density gradient contribution to $\overline{p\theta}$ is indispensable for ensuring proper van Driest scaling of fluctuations and mean velocity in the inertial sublayer. In the presence of wall heat transfer, proper modeling of $\overline{p\theta}$ might be needed to obtain the correct dependence of skin friction C_f on the wall temperature.[11]

Other explicit effects of compressibility includes the dilatational dissipation $\epsilon_s = (4/3)\nu\overline{\theta^2}$ (Refs. 6 and 12) which, studies have shown, must be included to obtain a growth rate (vs convective Mach number M_c) for compressible shear layers that agrees with experiments such as those of Papamoschu and Roshko.[13] Other roles have been attributed to ϵ_s in a turbulent boundary layer.[11] Underprediction of flow separation and overprediction of heat transfer rate near reattachment regions have been observed when the k–ϵ or k–ω model is used in complex supersonic and hypersonic flows.[2] Control of turbulence length scale was necessary to obtain reasonable results for these cases.

Aside from the fact that turbulence models on their own have not always worked well, we are finding out from our studies that the choice of numerical method might be a crucial factor for a successful implementation of a particular turbulence model. There are multi-

Received July 19, 1994; revision received Dec. 20, 1994; accepted for publication Dec. 27, 1994.

*Assistant Professor, Department of Mechanical Engineering. Member AIAA.

tudes of numerical schemes, with varying degrees of efficiency, and the choice among them is not an easy task. For example, options include the flux-difference split (FDS) schemes (such as those of Roe,[14] Harten and Lax,[15] and Rusanov[16]) and the flux-vector split (FVS) schemes,[17,18] as well as central-difference schemes.[19,20] Of these, Roe's method has been shown to be the most accurate and the one that gives the sharpest shock resolution.[21] For example, one-fifth to one-half as many points were required to resolve a shear layer using Roe's fluxes in a first-order scheme, compared to using other fluxes in second- or even third-order schemes. This would seem to be quite important, especially in three-dimensional flows, where a large payoff might be gained by the use of fewer points. However, all of the three schemes have defects. The basic Roe scheme could produce entropy-violating solutions,[22] and it has a slower convergence compared to FVS.[23] On the other hand, FVS tends to be too diffusive,[23] whereas the central difference schemes usually involve the explicit addition of dissipation—with the attendant issue of "how much is enough at a location."

Upwinding is pursued in this paper. Our approach combines the two flux-splitting schemes to utilize the best of these two methods; that is, faster convergence, in the case of FVS, whereas, for FDS, more accurate results and sharp resolution of shocks.[23–25] It is especially important to note that the hybrid scheme has a faster convergence than the fully FDS approach, for reasons explained in Simpson and Whitfield.[23] This scheme will be used in the framework of a node-implicit, finite volume, lower–upper procedure. We have been motivated to pursue this hybrid procedure by the excellent performance that has been observed on a variety of complex aerodynamic flows, including Euler and Navier–Stokes equations, steady and truely transient calculations, and stationary and dynamic grids.[1,23–25] However, the experience with this approach has been limited to laminar or eddy viscosity flows. A contribution of the present paper is the extension of the method to include the equations for the six components of Reynolds stress tensor plus an additional equation for turbulent dissipation. Models for the unclosed terms in the turbulence equations are presented, as are the extensions of the flux-splitting procedure to handle the moment equations. Results show accurate turbulence calculations when the numerical scheme is applied to zero pressure gradient turbulent boundary layer[5] and to a turbulent boundary layer experiencing the combined effects of an adverse pressure gradient, bulk compression, and concave streamline curvature.[26,27]

Finally, the paper by Lee et al.[4] is relevant to the present one, although there are significant differences. For example, we use the full three-dimensional Navier–Stokes equations, whereas Lee et al.[4] used the two-dimensional boundary-layer equations. Thus, we can potentially address more complicated geometries, such as those involving viscous/inviscid interaction and large curvature. The numerical methods are also different: marching (parabolic) approach in Lee et al.[4] but flux-splitting upwinding approach in the present calculations.

The mean equations are presented in Sec. II. This is followed in Sec. III by the turbulence closure models. The numerical procedure is contained in Sec. IV, results in Sec. V, and a summary of our work in Sec. VI.

II. Governing Equations

The mean flow equations, following Reynolds- and Favre-averaging procedures, can be written as

$$\frac{\partial \boldsymbol{q}}{\partial t} + \frac{\partial \boldsymbol{G}^k}{\partial x_k} = \frac{\partial \boldsymbol{G}_v{}^k}{\partial x_k} \tag{1}$$

where $\boldsymbol{q}$ is the vector of conserved variables, or

$$\boldsymbol{q} = \begin{bmatrix} \bar{\rho} \\ \bar{\rho}\tilde{u}_1 \\ \bar{\rho}\tilde{u}_2 \\ \bar{\rho}\tilde{u}_3 \\ \bar{\rho}\tilde{E} \end{bmatrix} \tag{2}$$

and $\boldsymbol{G}^k$ is the tensor of convective terms, which is given by

$$\boldsymbol{G}^k \equiv \begin{bmatrix} \boldsymbol{G}^1 & \boldsymbol{G}^2 & \boldsymbol{G}^3 \end{bmatrix} = \begin{bmatrix} \bar{\rho}\tilde{u}_1 & \bar{\rho}\tilde{u}_2 & \bar{\rho}\tilde{u}_3 \\ \bar{\rho}\tilde{u}_1\tilde{u}_1 + \bar{p} & \bar{\rho}\tilde{u}_1\tilde{u}_2 & \bar{\rho}\tilde{u}_1\tilde{u}_3 \\ \bar{\rho}\tilde{u}_1\tilde{u}_2 & \bar{\rho}\tilde{u}_2\tilde{u}_2 + \bar{p} & \bar{\rho}\tilde{u}_2\tilde{u}_3 \\ \bar{\rho}\tilde{u}_1\tilde{u}_3 & \bar{\rho}\tilde{u}_2\tilde{u}_3 & \bar{\rho}\tilde{u}_3\tilde{u}_3 + \bar{p} \\ \tilde{u}_1(\bar{\rho}\tilde{E} + \bar{p}) & \tilde{u}_2(\bar{\rho}\tilde{E} + \bar{p}) & \tilde{u}_3(\bar{\rho}\tilde{E} + \bar{p}) \end{bmatrix} \tag{3}$$

$\boldsymbol{G}_v^k$ is the tensor of diffusive terms,

$$\boldsymbol{G}_v^k \equiv \begin{bmatrix} \boldsymbol{G}_v^1 & \boldsymbol{G}_v^2 & \boldsymbol{G}_v^3 \end{bmatrix} = \begin{bmatrix} 0 & 0 & 0 \\ \bar{\sigma}_{11} + \tau_{11} & \bar{\sigma}_{12} + \tau_{12} & \bar{\sigma}_{13} + \tau_{13} \\ \bar{\sigma}_{21} + \tau_{21} & \bar{\sigma}_{22} + \tau_{22} & \bar{\sigma}_{23} + \tau_{23} \\ \bar{\sigma}_{31} + \tau_{31} & \bar{\sigma}_{32} + \tau_{32} & \bar{\sigma}_{33} + \tau_{33} \\ G_{v5,1} & G_{v5,2} & G_{v5,3} \end{bmatrix} \tag{4}$$

where

$$G_{v5,1} = u_1\bar{\sigma}_{11} + u_2\bar{\sigma}_{12} + u_3\bar{\sigma}_{13} - \bar{q}_1 - \overline{p''u_1''} + \overline{u_1''\sigma_{11}''} + \overline{u_2''\sigma_{12}''} + \overline{u_3''\sigma_{13}''} - \bar{\rho}\widetilde{E'u_1'}$$

$$G_{v5,2} = u_1\bar{\sigma}_{21} + u_2\bar{\sigma}_{22} + u_3\bar{\sigma}_{23} - \bar{q}_2 - \overline{p''u_2''} + \overline{u_1''\sigma_{21}''} + \overline{u_2''\sigma_{22}''} + \overline{u_3''\sigma_{23}''} - \bar{\rho}\widetilde{E'u_2'}$$

$$G_{v5,3} = u_1\bar{\sigma}_{31} + u_2\bar{\sigma}_{32} + u_3\bar{\sigma}_{33} - \bar{q}_3 - \overline{p''u_3''} + \overline{u_1''\sigma_{31}''} + \overline{u_2''\sigma_{32}''} + \overline{u_3''\sigma_{33}''} - \bar{\rho}\widetilde{E'u_3'}$$

In the preceding, an overbar indicates the mean relative to Reynolds averaging, with a double prime for the fluctuation. A tilde and a single prime are the corresponding notations for Favre-averaging. Also, x_i are the coordinate directions, t is time, ρ is density, u_i are the velocities in the three coordinate directions, and $\tilde{E}$ is total energy, with the turbulent energy flux $\widetilde{E'u_k'}$ defined as

$$\widetilde{E'u_k'} = C_v\widetilde{T'u_k'} + \tilde{u}_j\widetilde{u_k'u_j'} + (\widetilde{u_j'u_j'u_k'}/2) \tag{5}$$

Here, $\bar{p}$ is mean pressure. The equation of state is

$$\bar{p} = (\gamma - 1)\left[\bar{\rho}\tilde{E} - \tfrac{1}{2}\bar{\rho}\tilde{u}_i\tilde{u}_i - \tfrac{1}{2}\bar{\rho}\widetilde{u_i'u_i'}\right] \tag{6}$$

The mean viscous stress tensor $\bar{\sigma}_{ij}$ is approximated as

$$\bar{\sigma}_{ij} = \bar{\mu}\left(\frac{\partial\tilde{u}_i}{\partial x_j} + \frac{\partial\tilde{u}_j}{\partial x_i}\right) - \frac{2}{3}\bar{\mu}\frac{\partial\tilde{u}_k}{\partial x_k}\delta_{ij} \tag{7}$$

and $\bar{q}_k$ is the mean heat flux

$$q_k = -\kappa\frac{\partial\tilde{T}}{\partial x_k} \tag{8}$$

Finally, τ_{ij} is the Reynolds stress tensor, $\bar{\rho}\widetilde{u_i'u_j'}$.

III. Turbulence Models

The terms $-\bar{\rho}\widetilde{u_i'u_j'}$, $\overline{\sigma_{jk}''u_j''}$, $\overline{p''u_k''}$, $\widetilde{T'u_k'}$, and $\widetilde{u_j'u_j'u_k'}/2$ in the mean equations are not known or expressible in terms of the solution variables. Thus, models have to be given to assign values to them or to express them in terms of the solution variables. Reynolds- and Favre-averaged transport equations are solved for the Reynolds stress tensor, for which the equations are given by

$$\frac{\partial}{\partial t}(\bar{\rho}\widetilde{u_i'u_j'}) + \frac{\partial}{\partial x_k}(\bar{\rho}\tilde{u}_k\widetilde{u_i'u_j'}) = P_{ij} + \Pi_{ij} - \frac{\partial T_{ijk}}{\partial x_k} - \bar{\rho}\epsilon_{ij} + \frac{2}{3}\overline{p''\frac{\partial u_k''}{\partial x_k}}\delta_{ij} - \overline{u_i'}\frac{\partial\bar{p}}{\partial x_j} - \overline{u_j'}\frac{\partial\bar{p}}{\partial x_i} + \overline{u_i'}\frac{\partial\bar{\sigma}_{jk}}{\partial x_k} + \overline{u_j'}\frac{\partial\bar{\sigma}_{ik}}{\partial x_k} \tag{9}$$

where

$$P_{ij} = -\bar{\rho}\left(\widetilde{u_i'u_k'}\frac{\partial \tilde{u}_j}{\partial x_k} + \widetilde{u_j'u_k'}\frac{\partial \tilde{u}_i}{\partial x_k}\right)$$

$$\Pi_{ij} = \overline{p''\frac{\partial u_i''}{\partial x_j}} + \overline{p''\frac{\partial u_j''}{\partial x_i}} - \frac{2}{3}\overline{p''\frac{\partial u_k''}{\partial x_k}}\delta_{ij}$$

$$T_{ijk} = \bar{\rho}\widetilde{u_i'u_j'u_k'} + (\overline{p''u_i''}\delta_{jk} + \overline{p''u_j''}\delta_{ik}) - (\overline{\sigma_{ik}''u_j''} + \overline{\sigma_{ik}''u_j''})$$

$$\epsilon_{ij} = \overline{\sigma_{ik}''\frac{\partial u_j''}{\partial x_k}} + \overline{\sigma_{jk}''\frac{\partial u_i''}{\partial x_k}}$$

In Eq. (9), from left to right, we have the time rate of change of the Reynolds stress at a fixed point, the net convection of Reynolds stress by the mean flow to the fixed point, local production (P_{ij}) of Reynolds stress, local pressure strain (Π_{ij}), net diffusive transport ($T_{ijk,k}$) of Reynolds stress to the fixed point, local dissipation tensor, and local pressure dilatation. The last four terms are the "production" of Reynolds stress at the fixed point by Favre- (mass-) averaged velocity. In these equations, the following terms are closed: the time rate of change of the Reynolds stress, the convective term, and the production term. Whereas, the terms Π_{ij}, $T_{ijk,k}$, ϵ_{ij}, and the pressure dilation and the mass-averaged velocity terms are unclosed.

Some of the unclosed terms in these equations are modeled using the variable density extension of the incompressible models whereas explicit compressible models are required for others. More details are now provided on the various models used.

A. Solenoidal Dissipation and Dissipation Rate Equation

Sarkar et al.[28] and Zeman[12] have suggested that, for large Reynolds number compressible flows, dissipation ϵ consists of two parts,

$$\epsilon = \epsilon_s + \epsilon_d \tag{10}$$

where ϵ_s represents the solenoidal dissipation and ϵ_d represents the compressible dissipation,

$$\epsilon_s = \bar{\nu}\overline{\omega_i''\omega_i''}, \qquad \epsilon_d = \tfrac{4}{3}\bar{\nu}\overline{d''^2} \tag{11}$$

Here, $d'' \equiv u_{k,k}''$ is the fluctuating dilatation, and $\omega_i'' = \epsilon_{ijk}u_{k,j}''$ represents the fluctuating vorticity. The term ϵ_{ijk} is the permutation tensor. Models for ϵ_d are based on the assumption that compressible dissipation is a function of the turbulent Mach number. Zeman's approach assumes the existence of shock-like structures embedded within the energetic turbulent eddies, whereas Sarkar et al.[28] use low-Mach number asymptotics to obtain a scaling relation. With Sarkar et al.,[28] $\epsilon_d = M_t^2\epsilon_s$, where $M_t = q/c^2$ is the turbulent Mach number, c is the speed of sound $= \sqrt{\gamma\bar{p}/\bar{\rho}}$, and q is a velocity scale characteristic of turbulence (defined later). Zeman's model is more general as it incorporates intermittency and dependence on γ, the ratio of specific heats. One form of Zeman's model is

$$\epsilon_d = \epsilon_s c_d\left(1 - \exp\left\{-\left(\frac{M_{t^*} - M_{t_0}}{\sigma_M}\right)^2\right\}\right)$$

where $\epsilon_d = 0$ if $M_{t^*} \le M_{t_0}$, with $M_{t_0} = 0.2$, $\sigma_M = 0.66$, $c_d = 0.75$, and $M_{t^*} = \sqrt{[2/(\gamma+1)]}M_t$. The results presented here were obtained using the approach of Sarkar et al.[28]

The transport equation we have used for the solenoidal dissipation is based on a variable density extension of the incompressible model in Hanjalic and Launder[29]

$$\frac{\partial(\bar{\rho}\epsilon_s)}{\partial t} + \frac{\partial(\bar{\rho}\tilde{u}_k\epsilon_s)}{\partial x_k} = -C_{\epsilon 1}\frac{\epsilon_s}{k}\bar{\rho}\widetilde{u_i'u_j'}\frac{\partial \tilde{u}_i}{\partial x_j} - C_{\epsilon 2}\bar{\rho}\frac{\epsilon_s^2}{k}$$

$$+ \frac{\partial}{\partial x_k}\left(C_\epsilon\frac{\bar{\rho}k}{\epsilon_s}\widetilde{u_k'u_l'}\frac{\partial \epsilon_s}{\partial x_l}\right) \tag{12}$$

where the constants are $C_\epsilon = 0.18$, $C_{\epsilon 1} = 1.44$, and $C_{\epsilon 2} = 1.9$. Wall value for ϵ_s is $(\epsilon_s)_w = 2\nu(\partial k^{\frac{1}{2}}/\mathrm{d}y)^2$.

The model we have used for the dissipation rate tensor is[30]

$$\epsilon_{ij} = \bar{\rho}(\epsilon/k)\left[\widetilde{u_i'u_j'}f_s + \tfrac{2}{3}(1 - f_s)k\delta_{ij}\right] \tag{13}$$

where f_s is a function of the turbulent Reynolds number $R_t = k^2/\nu\epsilon$ and is given by $f_s = [10/(10 + R_t)]$. This model contracts to 2ϵ at the wall, meaning that it has the correct asymptotic behavior at the wall.

B. Pressure Strain

Many options exist for modeling the pressure-strain correlation (Π_{ij}) (Refs. 4, 31, and 32), but the more popular model by Launder, Reece, and Rodi[32] (LRR) is used. A model for the fast term by Lee et al.[4] might be more suitable as it incorporates the effect of Mach number. However, it has not been calibrated for many flows in comparison to the LRR models. The more simple isotropization of production (IP) model of LRR is used,

$$\Pi_{ij} = \underbrace{-C_1\bar{\rho}\epsilon b_{ij}}_{\text{slow term}} - \underbrace{C_2[P_{ij} - (P_{kk}/3)\delta_{ij}]}_{\text{fast term}} \equiv \Pi_{ij}^1 + \Pi_{ij}^2 \tag{14}$$

where b_{ij} is the anisotropy tensor, given by

$$b_{ij} = \left(\widetilde{u_i'u_j'}/q^2\right) - (\delta_{ij}/3) \tag{15}$$

and $q^2 = \widetilde{u_k'u_k'} = 2k$ denotes the trace of the Reynolds stress tensor. Here, k is kinetic energy of turbulence. We include wall (echo) effects in the pressure strain by assuming the model in Launder and Shima[33]

$$\Pi_{ij}^w = \left(\Pi_{ij}^{w,1} + \Pi_{ij}^{w,2}\right)f(l/y_n) \tag{16}$$

where the slow wall correction term Π_{ij}^{w1} is given by

$$\Pi_{ij}^{w,1} = C_1'(\epsilon\bar{\rho}/k)\left[\widetilde{u_k'u_m'}n_kn_m\delta_{ij} - (3/2)\left(\widetilde{u_k'u_i'}n_kn_j + \widetilde{u_k'u_j'}n_kn_i\right)\right] \tag{17}$$

and the fast wall correction term $\Pi_{ij}^{w,2}$ is given by

$$\Pi_{ij}^{w,2} = C_2'\left[\Pi_{km}^2n_kn_m\delta_{ij} - (3/2)\left(\Pi_{ik}^2n_kn_j + \Pi_{jk}^2n_kn_i\right)\right] \tag{18}$$

The near-wall damping function f is normalized to unity in the fully turbulent region of a turbulent boundary layer. The quantity y_n is the normal distance to the wall. The quantity l represents the turbulent length scale of the flow which is estimated to be

$$l = \left(k^{\frac{3}{2}}/\epsilon\right)$$

Launder and Shima have shown the near-wall damping function f to be

$$f(l/y_n) = 0.41\left(k^{\frac{3}{2}}/\epsilon y_n\right) \tag{19}$$

The constants C_1' and C_2' are $C_1' = 0.5$ and $C_2' = 0.3$.

C. Transport Terms

The transport term $T_{ijk,k}$ consists of three parts,

$$T_{ijk,k} = \underbrace{C_{ijk,k}}_{\text{turbulent diffusion}} + \underbrace{E_{ijk,k}}_{\text{pressure diffusion}} - \underbrace{D_{ijk,k}}_{\text{viscous diffusion}}$$

The model for the triple correlation, $(C_{ijk,k}) \equiv \bar{\rho}\widetilde{u_i'u_j'u_k'}$, is[29]

$$C_{ijk,k} = \frac{\partial}{\partial x_k}\left\{-C_s\bar{\rho}\frac{(q^2)^2}{\epsilon}\left[\frac{\partial(\widetilde{u_i'u_j'})}{\partial x_k} + \frac{\partial(\widetilde{u_j'u_k'})}{\partial x_i} + \frac{\partial(\widetilde{u_i'u_k'})}{\partial x_j}\right]\right\} \tag{20}$$

The model coefficient C_s is 0.018. We will assume that pressure diffusion effects are included in the model for the triple correlation, as did Hanjalic and Launder.[29] The various other models proposed

for pressure diffusion have not performed significantly better than the one used here.[34]

The viscous diffusion term is modeled according to Launder and Shima,[33] and is given by

$$D_{ijk,k} = \frac{\partial}{\partial x_k}\left(\bar{\mu}\frac{\partial \widetilde{u_i' u_j'}}{\partial x_k}\right) \tag{21}$$

D. Mass-Averaged Fluctuating Velocity

The Favre-averaging procedure introduces the quantity $\overline{u_i'}$, which does not appear in the incompressible form of the Reynolds transport equation. Gradient transport is assumed,

$$\overline{u_i'} = -\frac{\overline{\rho'' u_i''}}{\bar{\rho}} = \frac{C_\mu k^2}{\bar{\rho}\epsilon\sigma_p}\frac{\partial \bar{\rho}}{\partial x_i} \tag{22}$$

The model constant $C_\mu = 0.09$ is taken from Sarkar and Lakshmanan,[6] whereas the turbulent Schmidt number $\sigma_p = 0.7$.

E. Unclosed Terms in the Mean Energy Equation

The turbulent quantities that need to be closed in the mean energy equation are

$$\overline{\sigma_{jk}'' u_j''},\ \overline{p'' u_k''}, \qquad u_j'\widetilde{u_j' u_k'}/2, \qquad \widetilde{T' u_k'}$$

From the definition of the transport term in the Reynolds stress transport equation, the quantities $\overline{\sigma_{jk}'' u_j''}$, $\overline{p'' u_k''}$, and $u_j' u_j' u_k'/2$ can be combined to yield

$$\overline{\sigma_{jk}'' u_j''} - \overline{p'' u_k''} - (u_j'\widetilde{u_j' u_k'}/2) = -(T_{jjk}/2)$$

Thus the models in Sec. III.C are applicable.

Concerning $\widetilde{T' u_k'}$, evolution equations can be written[11] which introduce three additional transport equations. For simplicity, we are using a gradient transport[6] as

$$\widetilde{T' u_k'} = -\frac{C_\mu k^2}{\epsilon\sigma_T}\frac{\partial \tilde{T}}{\partial x_k} \tag{23}$$

where $\sigma_T = 0.7$ is the turbulence Prandtl number.

In this equation $\boldsymbol{q}_{rs}$ is the vector of the unknown stresses given by

$$\boldsymbol{q}_{rs} = \begin{bmatrix} \bar{\rho}\widetilde{u_1' u_1'} \\ \bar{\rho}\widetilde{u_1' u_2'} \\ \bar{\rho}\widetilde{u_1' u_3'} \\ \bar{\rho}\widetilde{u_2' u_2'} \\ \bar{\rho}\widetilde{u_2' u_3'} \\ \bar{\rho}\widetilde{u_3' u_3'} \\ \bar{\rho}\epsilon_s \end{bmatrix}$$

$\boldsymbol{G}_{rs}^k$ is the tensor of convective terms given by

$$\boldsymbol{G}_{rs}^k \equiv \left[\boldsymbol{G}_{rs}^1 \quad \boldsymbol{G}_{rs}^2 \quad \boldsymbol{G}_{rs}^3\right]$$

$$= \begin{bmatrix} \bar{\rho}\widetilde{u_1' u_1'}\tilde{u}_1 & \bar{\rho}\widetilde{u_1' u_1'}\tilde{u}_2 & \bar{\rho}\widetilde{u_1' u_1'}\tilde{u}_3 \\ \bar{\rho}\widetilde{u_1' u_2'}\tilde{u}_1 & \bar{\rho}\widetilde{u_1' u_2'}\tilde{u}_2 & \bar{\rho}\widetilde{u_1' u_2'}\tilde{u}_3 \\ \bar{\rho}\widetilde{u_1' u_3'}\tilde{u}_1 & \bar{\rho}\widetilde{u_1' u_3'}\tilde{u}_2 & \bar{\rho}\widetilde{u_1' u_3'}\tilde{u}_3 \\ \bar{\rho}\widetilde{u_2' u_2'}\tilde{u}_1 & \bar{\rho}\widetilde{u_2' u_2'}\tilde{u}_2 & \bar{\rho}\widetilde{u_2' u_2'}\tilde{u}_3 \\ \bar{\rho}\widetilde{u_2' u_3'}\tilde{u}_1 & \bar{\rho}\widetilde{u_2' u_3'}\tilde{u}_2 & \bar{\rho}\widetilde{u_2' u_3'}\tilde{u}_3 \\ \bar{\rho}\widetilde{u_3' u_3'}\tilde{u}_1 & \bar{\rho}\widetilde{u_3' u_3'}\tilde{u}_2 & \bar{\rho}\widetilde{u_3' u_3'}\tilde{u}_3 \\ \bar{\rho}\epsilon_s\tilde{u}_1 & \bar{\rho}\epsilon_s\tilde{u}_2 & \bar{\rho}\epsilon_s\tilde{u}_3 \end{bmatrix}$$

$\boldsymbol{S}_{rs1}$ and $\boldsymbol{S}_{rs2}$ are source vectors given by

$$\boldsymbol{S}_{rs1} = \begin{bmatrix} P_{11} + \Pi_{11} - \epsilon_{11} + \Pi_{11}^w \\ P_{12} + \Pi_{12} - \epsilon_{12} + \Pi_{12}^w \\ P_{13} + \Pi_{13} - \epsilon_{13} + \Pi_{13}^w \\ P_{22} + \Pi_{22} - \epsilon_{22} + \Pi_{22}^w \\ P_{23} + \Pi_{23} - \epsilon_{23} + \Pi_{23}^w \\ P_{33} + \Pi_{33} - \epsilon_{33} + \Pi_{33}^w \\ -C_{\epsilon 1}\dfrac{\epsilon_s}{k}\left(\dfrac{P_{11} + P_{22} + P_{33}}{2}\right) - C_{\epsilon 2}\bar{\rho}\dfrac{\epsilon_s}{k} \end{bmatrix}$$

$$\boldsymbol{S}_{rs1} = \begin{bmatrix} \overline{u_1'}(\bar{\sigma}_{11,1} + \bar{\sigma}_{12,2} + \bar{\sigma}_{13,3}) - \overline{u_1'}\dfrac{\partial \bar{p}}{\partial x} + \overline{u_1'}(\bar{\sigma}_{11,1} + \bar{\sigma}_{12,2} + \bar{\sigma}_{13,3}) - \overline{u_1'}\dfrac{\partial \bar{p}}{\partial x} \\ \overline{u_1'}(\bar{\sigma}_{21,1} + \bar{\sigma}_{22,2} + \bar{\sigma}_{23,3}) - \overline{u_1'}\dfrac{\partial \bar{p}}{\partial y} + \overline{u_2'}(\bar{\sigma}_{11,1} + \bar{\sigma}_{12,2} + \bar{\sigma}_{13,3}) - \overline{u_2'}\dfrac{\partial \bar{p}}{\partial x} \\ \overline{u_1'}(\bar{\sigma}_{31,1} + \bar{\sigma}_{32,2} + \bar{\sigma}_{33,3}) - \overline{u_1'}\dfrac{\partial \bar{p}}{\partial z} + \overline{u_3'}(\bar{\sigma}_{11,1} + \bar{\sigma}_{12,2} + \bar{\sigma}_{13,3}) - \overline{u_3'}\dfrac{\partial \bar{p}}{\partial x} \\ \overline{u_2'}(\bar{\sigma}_{21,1} + \bar{\sigma}_{22,2} + \bar{\sigma}_{23,3}) - \overline{u_2'}\dfrac{\partial \bar{p}}{\partial y} + \overline{u_2'}(\bar{\sigma}_{21,1} + \bar{\sigma}_{22,2} + \bar{\sigma}_{23,3}) - \overline{u_2'}\dfrac{\partial \bar{p}}{\partial y} \\ \overline{u_2'}(\bar{\sigma}_{31,1} + \bar{\sigma}_{32,2} + \bar{\sigma}_{33,3}) - \overline{u_2'}\dfrac{\partial \bar{p}}{\partial z} + \overline{u_3'}(\bar{\sigma}_{21,1} + \bar{\sigma}_{22,2} + \bar{\sigma}_{23,3}) - \overline{u_3'}\dfrac{\partial \bar{p}}{\partial y} \\ \overline{u_3'}(\bar{\sigma}_{11,1} + \bar{\sigma}_{12,2} + \bar{\sigma}_{13,3}) - \overline{u_3'}\dfrac{\partial \bar{p}}{\partial z} + \overline{u_3'}(\bar{\sigma}_{31,1} + \bar{\sigma}_{32,2} + \bar{\sigma}_{33,3}) - \overline{u_3'}\dfrac{\partial \bar{p}}{\partial z} \\ 0 \end{bmatrix}$$

F. Pressure Dilatation

The model used in our code for $\overline{p\theta}$ is taken from Zeman.[11] However, for the calculations presented in this paper, $\overline{p\theta}$ effects are not significant and are omitted in the governing equations given subsequently. A more significant role of $\overline{p\theta}$ is expected at higher Mach numbers and/or larger heat fluxes than those considered in this paper.

With the foregoing, the final form of the turbulence equations can be written as

$$\frac{\partial \boldsymbol{q}_{rs}}{\partial t} + \frac{\partial \boldsymbol{G}_{rs}^k}{\partial x_k} = \boldsymbol{S}_{rs1} + \boldsymbol{S}_{rs2} + \frac{\partial \boldsymbol{D}_{rs}^k}{\partial x_k} \tag{24}$$

and $\boldsymbol{D}_{rs}^k$ is the tensor of diffusive terms

$$\boldsymbol{D}_{rs}^k = \left[\boldsymbol{D}_{rs}^1 \quad \boldsymbol{D}_{rs}^2 \quad \boldsymbol{D}_{rs}^3\right] = \begin{bmatrix} -T_{111} & -T_{112} & -T_{113} \\ -T_{121} & -T_{122} & -T_{123} \\ -T_{131} & -T_{132} & -T_{133} \\ -T_{221} & -T_{222} & -T_{223} \\ -T_{231} & -T_{232} & -T_{233} \\ -T_{331} & -T_{332} & -T_{333} \\ D_{rs7,1} & D_{rs7,1} & D_{rs7,3} \end{bmatrix}$$

where

$$D_{rs7,1} = C_\epsilon \frac{\bar{\rho}k}{\epsilon_s}\left(\widetilde{u_1'u_1'}\frac{\partial \epsilon_s}{\partial x} + \widetilde{u_1'u_2'}\frac{\partial \epsilon_s}{\partial y} + \widetilde{u_1'u_3'}\frac{\partial \epsilon_s}{\partial z}\right)$$

$$D_{rs7,2} = C_\epsilon \frac{\bar{\rho}k}{\epsilon_s}\left(\widetilde{u_1'u_2'}\frac{\partial \epsilon_s}{\partial x} + \widetilde{u_2'u_2'}\frac{\partial \epsilon_s}{\partial y} + \widetilde{u_2'u_3'}\frac{\partial \epsilon_s}{\partial z}\right)$$

$$D_{rs7,3} = C_\epsilon \frac{\bar{\rho}k}{\epsilon_s}\left(\widetilde{u_1'u_3'}\frac{\partial \epsilon_s}{\partial x} + \widetilde{u_2'u_3'}\frac{\partial \epsilon_s}{\partial y} + \widetilde{u_3'u_3'}\frac{\partial \epsilon_s}{\partial z}\right)$$

Initial conditions and boundary conditions will be discussed under specific sample calculations.

IV. Numerical Procedure

A cell-centered finite volume formulation is used, where the vector of dependent variables $\boldsymbol{q}$ or $\boldsymbol{q}_{rs}$ is assumed to "reside" at the centroid of the cell. Following the finite volume procedures, we can discretize Eq. (1) as

$$\Delta \boldsymbol{q}^n + \frac{\Delta t}{V}\sum_{l=1}^{6}(\boldsymbol{F}^{n+1}S)_l = \frac{\Delta t}{V}\sum_{l=1}^{6}\left(\boldsymbol{F}_v^{n+1}S\right)_l \tag{25}$$

where $\Delta \boldsymbol{q}^n = \boldsymbol{q}^{n+1} - \boldsymbol{q}^n$, $\boldsymbol{F} \equiv \boldsymbol{G}^k n^k$, $\boldsymbol{F}_v \equiv \boldsymbol{G}_v^k n^k$, and S is the area of a cell face, with an outward normal, n^k.

Beam and Warming[35] linearization gives

$$\boldsymbol{F}^{n+1} = \boldsymbol{F}^n + (\boldsymbol{A}\Delta \boldsymbol{q})^n + \mathcal{O}(\Delta t^2) \tag{26}$$

In the FDS scheme, the exact Jacobian of the Roe matrix is expensive to compute whereas approximated Jacobians have been observed to give poor convergence, compared to FVS.[23] In the present work, the FVS scheme is used to evaluate the Jacobians in the implicit part (left-hand side) of the matrix equation (31). The Euler flux $\boldsymbol{F}^n$ in the residual part (right-hand side) is computed using the FDS scheme.

For the FVS technique,

$$(\boldsymbol{F}^{\pm})^{n+1} = (\boldsymbol{F}^{\pm})^n + (\boldsymbol{A}^{\pm}\Delta \boldsymbol{q})^n \tag{27}$$

where the plus and minus signs indicate evaluation based on the positive and negative eigenvalues of matrix $(\boldsymbol{A})$, respectively. In terms of the centroid values, surface quantities are approximated, as an example, by

$$(\boldsymbol{A}\Delta \boldsymbol{q})^n_{i+\frac{1}{2},j,k} = (\boldsymbol{A}^+\Delta \boldsymbol{q})^n_{i,j,k} + (\boldsymbol{A}^-\Delta \boldsymbol{q})^n_{i+1,j,k} \tag{28}$$

The diffusive fluxes do not contain information on wave propagation. Therefore, the upwinding structure of the split (Euler) matrices will be destroyed if the diffusive terms are treated implicitly. Thus, they are linearized as

$$\boldsymbol{F}_v^{n+1} = \boldsymbol{F}_v^n + \mathcal{O}(\Delta t) \tag{29}$$

and treated explicitly, to preserve the upwinding scheme. For high-Reynolds number flows, Gatlin[36] has shown that this linearization is stable for CFL numbers to as high as 15.

For FDS via Roe splitting,[37] the flux at the surface is evaluated as

$$\boldsymbol{F}^n \equiv \boldsymbol{F} = \frac{\boldsymbol{F}_{i,j,k} + \boldsymbol{F}_{i+1,j,k}}{2} - \frac{1}{2}\sum_1^5 \alpha_k|\lambda_k|\boldsymbol{R}_k \tag{30}$$

Here, λ_k are the characteristic wave speeds of the Riemann problem and α_k represent the projection of $\Delta \boldsymbol{q}$ onto the eigenvectors of Roe's approximate Jacobian. $\boldsymbol{R}_k$ are the right eigenvectors of Roe's matrix. The fluxes $\boldsymbol{F}_{i+1,j,k}$, and $\boldsymbol{F}_{i,j,k}$ and in Eq. (30) are evaluated using the conserved variables $\boldsymbol{q}_{i+1,j,k}$ and $\boldsymbol{q}_{i,j,k}$, respectively. Following Frink,[38] the sum $\sum_1^5 \alpha_k|\lambda_k|\boldsymbol{R}_k$ is written in terms of five flux jumps, $\Delta \boldsymbol{F}_k$, each associated with a distinct eigenvalue $\tilde{\lambda}_k$ of Roe's matrix. In our procedure, the mean flow equations are segregated from the turbulence equations. That is, at a time step we first solve the (5×5) matrix system for the mean flow variables at a node, for all nodes in the mesh. We then follow with the solution of the (7×7) system for the turbulence equations before proceeding to the next time step. LU decomposition of the mean flow equations, using the two-pass algorithm gives the following.

1) Forward sweep:

$$\begin{aligned}&\left[\boldsymbol{I} + (\Delta t/V)\left((\boldsymbol{A}^+)^n_{i,j,k}S_{i+\frac{1}{2},j,k}\cdot + (\boldsymbol{A}^+)^n_{i,j,k}S_{i,j+\frac{1}{2},k}\right.\right.\\ &\quad\cdot + (\boldsymbol{A}^+)^n_{i,j,k}S_{i,j,k+\frac{1}{2}}\cdot + (\boldsymbol{A}^+)^n_{i-1,j,k}S_{i-\frac{1}{2},j,k}\\ &\quad\left.\left.\cdot + (\boldsymbol{A}^+)^n_{i,j-1,k}S_{i,j-\frac{1}{2},k}\cdot + (\boldsymbol{A}^+)^n_{i,j,k-1}S_{i,j,k-\frac{1}{2}}\cdot\right)\right]\Delta \boldsymbol{w}^n\\ &\quad = -(\Delta t/V)\boldsymbol{R}^n\end{aligned} \tag{31}$$

where

$$\boldsymbol{R}^n = -\frac{\Delta t}{V}\left(\sum_{l=1}^{6}(\boldsymbol{F}^n S)_l - \sum_{l=1}^{6}\left(\boldsymbol{F}_v^n S\right)_l\right) \tag{32}$$

and $[\cdot]$ indicates that, for example, the term $(\boldsymbol{A}^+)^n_{i-1,j,k}S_{i-\frac{1}{2},j,k}$ operates on $(\Delta \boldsymbol{q}^n)_{i-1,j,k}$. The unknown in this equation is $\Delta \boldsymbol{w}$, which is obtained by solving a sparse block lower tridiagonal matrix with forward substitution. Because boundary conditions are treated explicitly, $\Delta \boldsymbol{w}^n$ is set to zero at the left and bottom boundaries of the domain.

2) Backward sweep:

$$\begin{aligned}&\left[\boldsymbol{I} + (\Delta t/V)\left((\boldsymbol{A}^-)^n_{i,j,k}S_{i-\frac{1}{2},j,k}\bullet + (\boldsymbol{A}^-)^n_{i,j,k}S_{i,j-\frac{1}{2},k}\right.\right.\\ &\quad\cdot + (\boldsymbol{A}^-)^n_{i,j,k}S_{i,j,k-\frac{1}{2}}\cdot + (\boldsymbol{A}^-)^n_{i+1,j,k}S_{i+\frac{1}{2},j,k}\\ &\quad\left.\left.\cdot + (\boldsymbol{A}^-)^n_{i,j+1,k}S_{i,j+\frac{1}{2},k}\cdot + (\boldsymbol{A}^-)^n_{i,j,k+1}S_{i,j,k+\frac{1}{2}}\cdot\right)\right]\Delta \boldsymbol{q}^n\\ &\quad = \Delta W^n\end{aligned} \tag{33}$$

In Eq. (33), a sparse upper tridiagonal matrix is solved using backward substitution. At the right and top boundaries of the domain, $\Delta \boldsymbol{q}^n$ is set to zero for the same reason given earlier.

3) Update solution:

$$\boldsymbol{q}^{n+1} = \boldsymbol{q}^n + \Delta \boldsymbol{q}^n \tag{34}$$

For the turbulence equations, the analogous equations to Eqs. (31), (33), and (34) are

1) Forward sweep:

$$\begin{aligned}&\left[\boldsymbol{I} + (\Delta t/V)\left((\boldsymbol{A}_{rs}^+)^n_{i,j,k}S_{i+\frac{1}{2},j,k}\cdot + (\boldsymbol{A}_{rs}^+)^n_{i,j,k}S_{i,j+\frac{1}{2},k}\right.\right.\\ &\quad\cdot + (\boldsymbol{A}_{rs}^+)^n_{i,j,k}S_{i,j,k+\frac{1}{2}}\cdot + (\boldsymbol{A}_{rs}^+)^n_{i-1,j,k}S_{i-\frac{1}{2},j,k}\\ &\quad\left.\left.\cdot + (\boldsymbol{A}_{rs}^+)^n_{i,j-1,k}S_{i,j-\frac{1}{2},k}\cdot + (\boldsymbol{A}_{rs}^+)^n_{i,j,k-1}S_{i,j,k-\frac{1}{2}}\cdot\right)\right]\Delta \boldsymbol{w}_{rs}^n\\ &\quad = (\Delta t/V)\boldsymbol{R}_{rs}^n\end{aligned} \tag{35}$$

where

$$\begin{aligned}\boldsymbol{R}_{rs}^n = \frac{\Delta t}{V}\left(\sum_{l=1}^{6}\left(\boldsymbol{E}_{rs}^n S\right)_l - \sum_{l=1}^{6}\left((\boldsymbol{F}_{rs}^+)^n S\right)_l - \sum_{l=1}^{6}\left((\boldsymbol{F}_{rs}^-)^n S\right)_l\right.\\ \left. + S_{rs1}^n V + S_{rs2}^n V\right)\end{aligned} \tag{36}$$

2) Backward sweep:

$$\begin{aligned}&\left[\boldsymbol{I} + (\Delta t/V)\left((\boldsymbol{A}_{rs}^-)^n_{i,j,k}S_{i-\frac{1}{2},j,k}\cdot + (\boldsymbol{A}_{rs}^-)^n_{i,j,k}S_{i,j-\frac{1}{2},k}\right.\right.\\ &\quad\cdot + (\boldsymbol{A}_{rs}^-)^n_{i,j,k}S_{i,j,k-\frac{1}{2}}\cdot + (\boldsymbol{A}_{rs}^-)^n_{i+1,j,k}S_{i+\frac{1}{2},j,k}\\ &\quad\left.\left.\cdot + (\boldsymbol{A}_{rs}^-)^n_{i,j+1,k}S_{i,j+\frac{1}{2},k}\cdot + (\boldsymbol{A}_{rs}^-)^n_{i,j,k+1}S_{i,j,k+\frac{1}{2}}\cdot\right)\right]\Delta \boldsymbol{q}_{rs}^n\\ &\quad = \Delta \boldsymbol{w}_{rs}^n\end{aligned} \tag{37}$$

3) Update solution:

$$q_{rs}^{n+1} = q_{rs}^{n} + \Delta q_{rs}^{n} \tag{38}$$

V. Results

The performance of the schemes presented in this paper was investigated extensively by comparing the calculations with known benchmarks for laminar and turbulent flows. For laminar tests we calculated the shock tube problem and supersonic laminar boundary-layer flow. The benchmark input conditions in Sod[39] were used for the shock tube tests, and the three coordinate directions were tested, one coordinate at a time. Excellent agreement was found in comparison with the results obtained by Steger and Warming[18] and by Roe,[40] as the results lie on the same curves (Fig. 1). The present schemes seem to give accurate calculations compared with the various finite difference schemes investigated in Sod.[39] For example, whereas the MacCormack and Lax-Wendroff schemes produce oscillations behind the shock and shock transition occupies about 10 cells, in the present work the shock occupies roughly 3–5 cells with no oscillations.

We also compared our calculation of Carter's problem (Shakib[41]) for laminar supersonic flow over a flat plate at $M_\infty = 3$ with Carter's own calculations and the finite element calculations by Shakib.[41] The agreement was excellent for the quantities compared. The motivation for the laminar tests of our code was not to validate the schemes used, since this has been done elsewhere,[1,23–25] but to detect programming errors and build confidence in the procedures. The code was subsequently validated for second-moment calculations, as described subsequently.

The compressible turbulent flow over a flat plate was one of the problems chosen to validate our code for turbulent calculations. We compare our results with those by Spina and Smits,[6] who carried out a fundamental study of this problem, using experimental measurements. The Reynolds number per unit length, Re/m, is 6.5×10^7, and $M_\infty = 2.87$. Mean flow and turbulence data along the plate are available in Ref. 42.

The dynamic viscosity is assumed to depend only on temperature, and to obey the Sutherland law:

$$\tilde{\mu} = S_\mu \tilde{T}^{\frac{3}{2}}/(\tilde{T} + 110) \tag{39}$$

The constant $S_\mu = 1.454 \times 10^{-6}$ is based on the value of μ at a temperature of 100 K.

The boundary conditions for this problem are as follows.

Upstream:

$$(x = 0, y)$$

$$\bar{\rho} = 0.8478 \text{ kg/m}^3$$

$$\bar{\rho}\tilde{u}_1 = 479 \text{ kg/m}^2\text{s}$$

$$\bar{\rho}\tilde{u}_2 = 0 \text{ kg/m}^2\text{s}$$

$$\bar{\rho}\tilde{E} = 193{,}988.13 \text{ N/m}^2$$

$$\bar{\rho}\widetilde{u_i'u_j'} = 0 \text{ N/m}^2$$

$$\bar{\rho}\epsilon_s = 0 \text{ kg/ms}^3$$

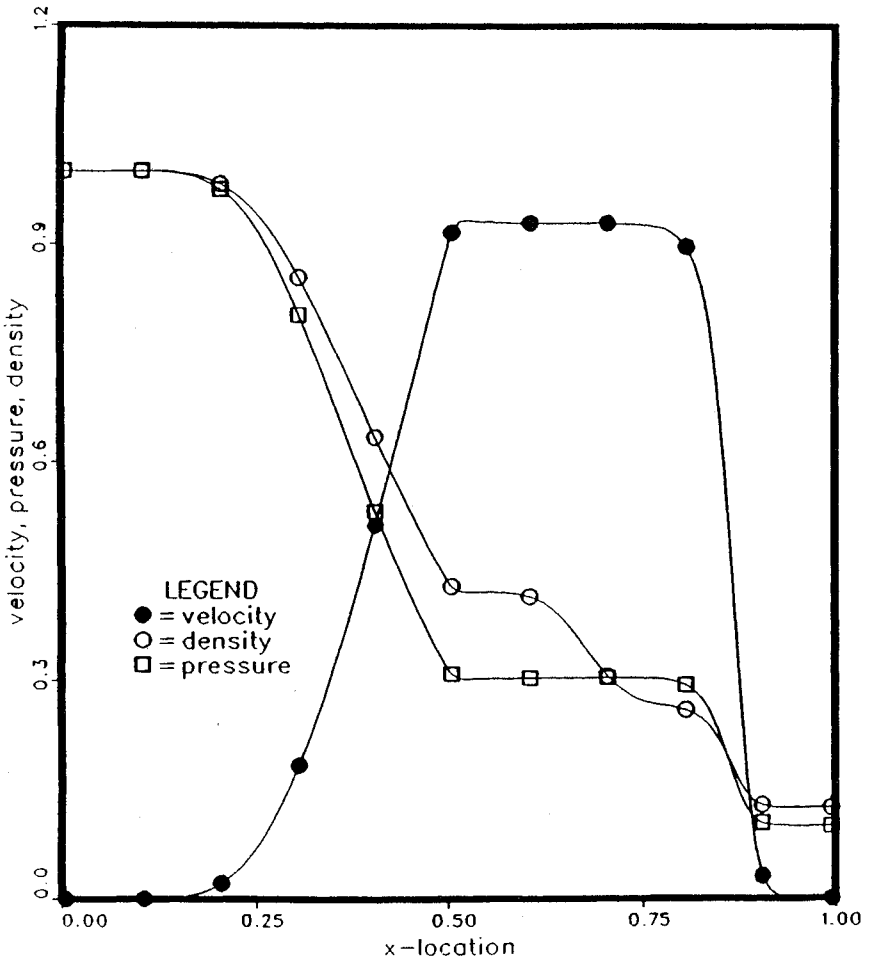

Fig. 1 Shock tube test problem showing the distribution of velocity u, density ρ, and pressure p; symbols are the computed results, solid lines are the correct benchmark solutions in Sod.[39]

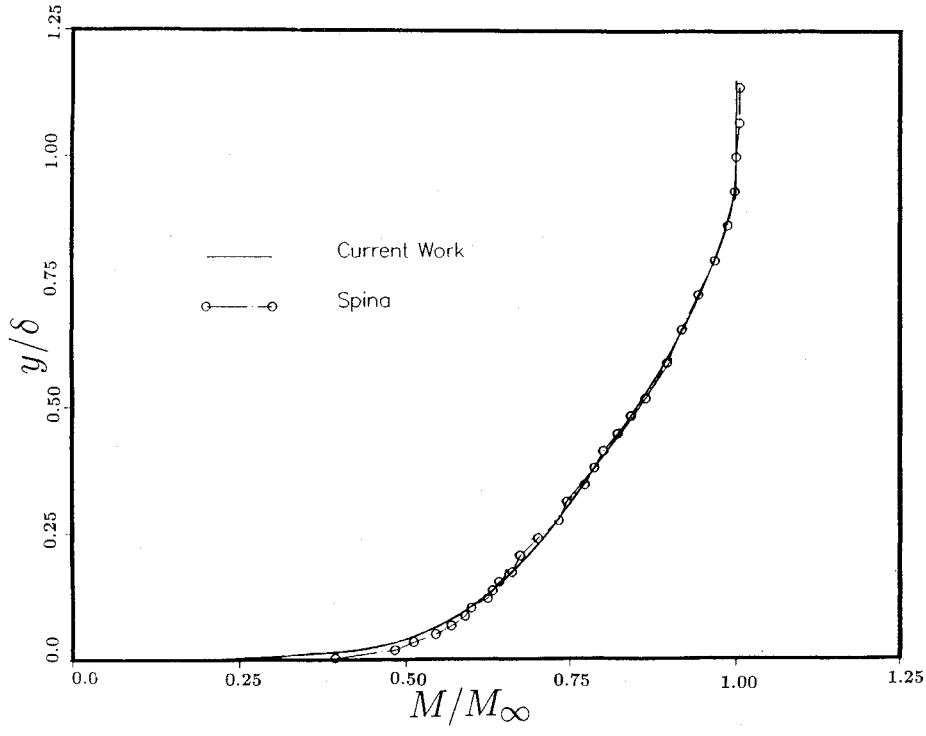

Fig. 2 Profile of mean Mach number for supersonic turbulent boundary layer flow with zero pressure gradient.

Plate:

$$(0 < x < 0.5, y = 0)$$

$$\frac{\partial \bar{\rho}}{\partial y} = 0 \text{ kg/m}^4$$

$$\bar{\rho}\tilde{u}_1 = 0 \text{ kg/m}^2\text{s}$$

$$\bar{\rho}\tilde{u}_2 = 0 \text{ kg/m}^2\text{s}$$

$$\bar{q} = 0 \text{ W/m}^2$$

$$\frac{\partial \bar{\rho}\tilde{E}}{\partial y} = 0 \text{ N/m}^3$$

$$\bar{\rho}\widetilde{u_i'u_j'} = 0 \text{ N/m}^2$$

$$\epsilon_s = 2\nu\left(\frac{\partial\sqrt{k}}{\partial y}\right)^2 \text{ m}^2/\text{s}^3$$

Finally, the condition of zero normal gradients of the conserved variables is specified at the freestream and downstream boundaries.

As is often the case in near-wall turbulence calculations, numerical experiments were needed to determine the grid required to resolve the viscous sublayer, $y^+ = \bar{\rho}_{\text{wall}} u_\tau / \mu_{\text{wall}} \leq 30$ (where the friction velocity $u_\tau = \sqrt{\sigma_{\text{wall}}/\bar{\rho}_{\text{wall}}}$) and the cell aspect ratio $S_{i+\frac{1}{2},j,k}/S_{i,j+\frac{1}{2},k}$ for stable calculations. For the various turbulence calculations, we observed very good convergence when 1) the centroid of the first cell along the plate is located such that $y^+ \sim 1$, 2) approximately 25 cells are used below $y^+ = 50$, and 3) cell aspect ratio is as large as 2500. With the proper initial conditions (next paragraph), the calculations are fairly insensitive to the grid used. The mesh used for this test consists of 171 grid points in the x direction and 71 exponentially varying grid points in the y direction. The centroid of the first cell along the plate is located at $y^+ \sim 0.35$.

Concerning initial conditions, a generalization of the procedure reported for k–ϵ models by Gerolymos[43] is used. Our procedure consists of estimating initial mean velocity profile between $y = 0$ and $y = \delta$ by using the $\frac{1}{7}$ power law, estimating initial mean density from Crocco's theorem, and using equilibrium conditions in Demuren and Sarkar[44] to determine initial stress levels. This seems to work very well. The initial external turbulence intensity is assumed to be 0.1%.

We compared the results at locations $x = 0.3$ m and $x = 0.5$ m along the plate and find the differences to be small; results are presented for $x = 0.5$ m.

The behavior of the boundary layer in the mean is compared in Figs. 2 and 3 for the profiles of the Mach number and mass flux ($\bar{\rho}\tilde{u}_1/\bar{\rho}_\infty\tilde{u}_{1,\infty}$). Agreement between the present work and experimental results is evident. Next, the velocity profile is mapped into the incompressible plane with the van Driest transformation[45] or

$$u^+ = \frac{1}{A\sqrt{(C_f/2)(\tilde{T}_w/\tilde{T}_e)}}\left[\sin^{-1}\left(\frac{2A^2\tilde{u}_1/\tilde{u}_{1,e} - B}{\sqrt{B^2+4A^2}}\right) + \sin^{-1}\left(\frac{B}{\sqrt{B^2+4A^2}}\right)\right] \tag{40}$$

where

$$A^2 = \frac{\tilde{T}_e}{\tilde{T}_w}\left(\frac{\gamma-1}{2}\right)M_e^2, \qquad B = \frac{\tilde{T}_e}{\tilde{T}_w} + A^2 - 1$$

The subscripts e and w refer to properties taken at the edge of the boundary layer and at the wall, respectively. Figure 4, which contains the log-law plot at $x = 0.5$ m, shows a very good agreement with the experimental results of Spina.

In Fig. 5 we present the computed near-wall energy budget (again at $x = 0.5$ m), nondimensionalized by $\bar{\rho}u_\tau^4/\bar{\nu}_{\text{wall}}$. The calculations agree with those reported by Grasso and Falconi.[46] Further, we calculated an approximate value of 0.3 across the boundary layer for the structural parameter $a^* = -\widetilde{u_1'u_2'}/\widetilde{u_1'u_1'}$. This value is essentially the same as that reported by Jayaram et al.[26] for the upstream (zero pressure gradient) portion of a Mach 2.87 turbulent boundary layer over a concave surface curvature (see next paragraph).

As a final demonstration of the potential usefulness of the procedures presented in this paper we will discuss the calculation of a supersonic turbulent boundary layer experiencing the combined effects of an adverse pressure gradient, bulk compression, and concave streamline curvature.[26,27] These effects result from flows over

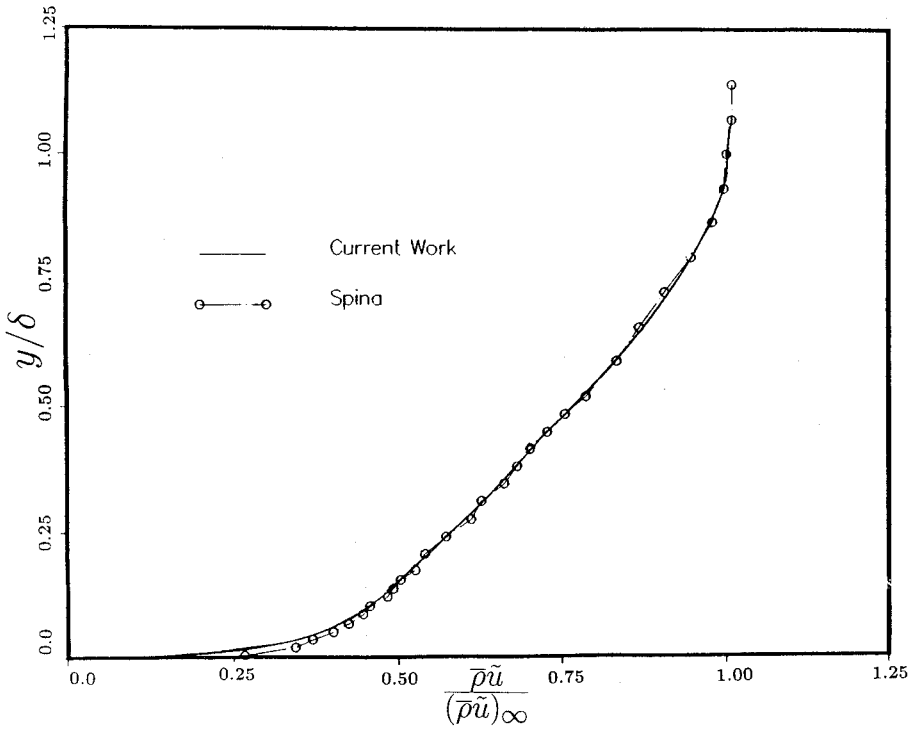

Fig. 3 Profile of mass flux $\bar{\rho}\tilde{u}_1/\bar{\rho}\tilde{u}_{1,\infty}$ for supersonic turbulent boundary layer flow with zero pressure gradient.

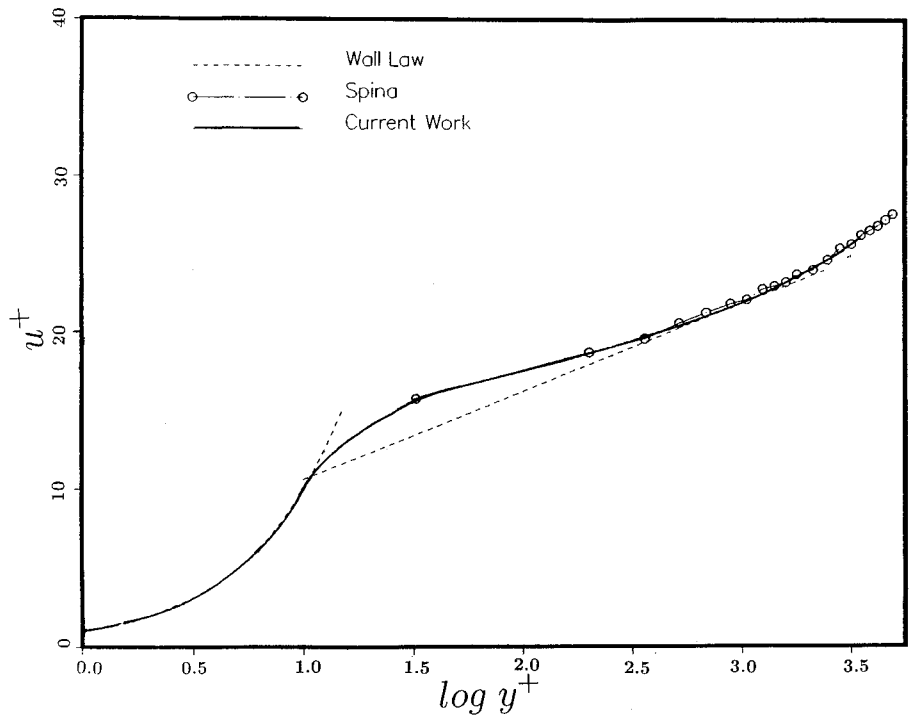

Fig. 4 Profile of log-law velocity u^+ after Van Driest transformation, for supersonic turbulent boundary layer flow with zero pressure gradient.

short regions of concave surface curvature. The upstream of the ramp consists of a Mach 2.87 boundary layer with a thickness of $\delta = 0.025$ m. The total pressure is 6.9×10^5 N/m^2 and the Reynolds number is 6.3×10^7/m. The strong adverse pressure gradient case in which boundary-layer thickness-to-curvature ratio (δ/R_c) is 0.1 is calculated.

The predictions are compared with experimental measurements in Figs. 6–9, where we show the wall pressure p_w/p_∞ and skin friction C_f as functions of x/δ, and the normal stress $\bar{\rho}\widetilde{u'^2}/\bar{\rho}_\infty\tilde{u}_\infty^2$ and the shear stress $-\bar{\rho}\widetilde{u'v'}/\bar{\rho}_\infty\tilde{u}_\infty^2$ as functions of y/δ for $x/\delta \approx 0.5$, 1, and 2. The predicted results for the various quantities compared show reasonable agreement with the experimental measurements. The exception is the shear stress result for $x/\delta \approx 2$, $y/\delta < 0.8$, where a significant deviation can be observed. The precise cause of the disparity is not known, but it does not appear to be numerical. Finally, comparisons were drawn between the present work and those in Lee et al.,[4] in the introductory section of this paper. We will like to point out that, relative to the experimental measurements, the pressure and skin friction results from our calculations are better than those reported by Lee et al., although more studies are needed for a conclusive statement. For reasons of space, the comparison exercise is not presented; the interested reader can make the assessment by comparing our results with the published work of Lee et al.

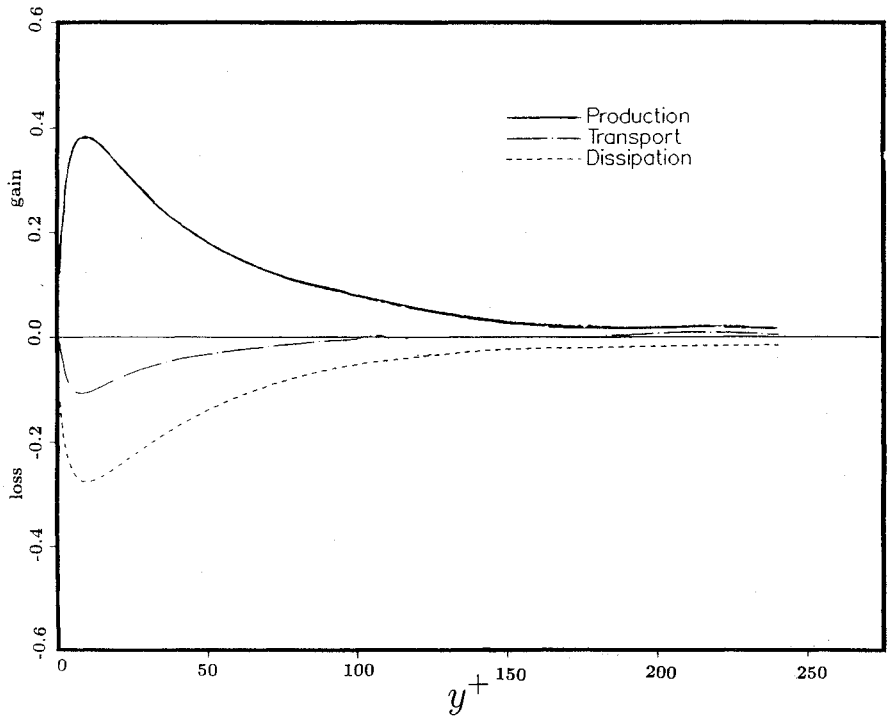

Fig. 5 Near-wall energy budget for supersonic turbulent boundary layer flow with zero pressure gradient.

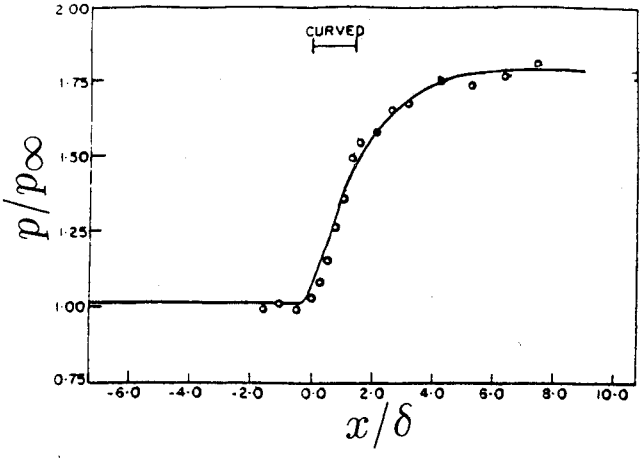

Fig. 6 Normalized wall pressure as a function of x for supersonic turbulent flow over a ramp; symbols are experimental measurements, solid lines are computed results.

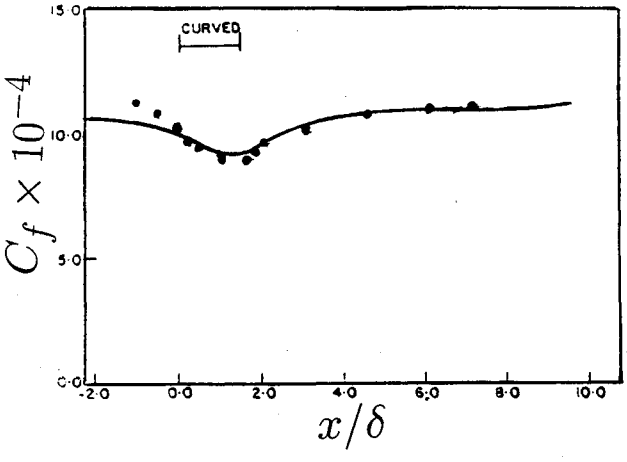

Fig. 7 Skin friction as a function of x for supersonic turbulent flow over a ramp; symbols are experimental measurements, solid lines are computed results.

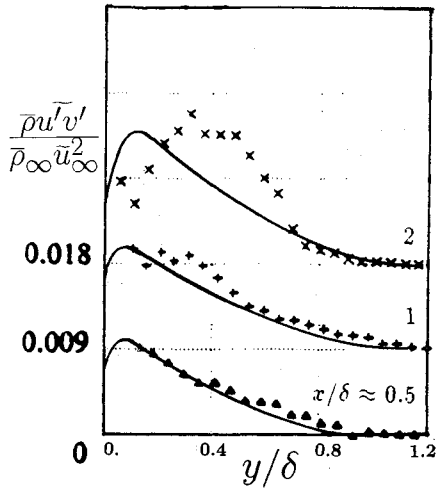

Fig. 8 Normalized shear stress as a function of x/δ and y/δ for supersonic turbulent flow over a ramp; symbols are experimental measurements, solid lines are computed results.

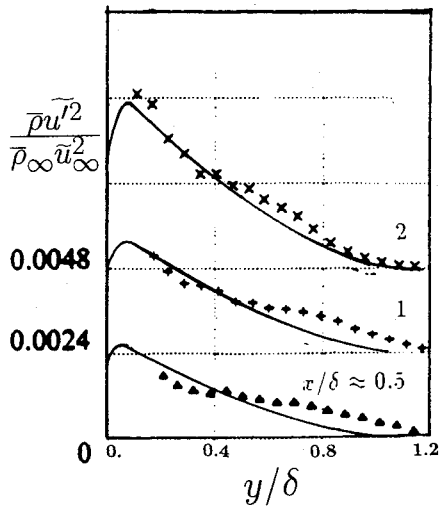

Fig. 9 Normalized shear stress as a function of x/δ and y/δ for supersonic turbulent flow over a ramp; symbols are experimental measurements, solid lines are computed results.

A. Computing Performance

For turbulence calculations involving the mean flow equations, the six equations for the second moments, and an additional one for dissipation, speed of computation is 0.00394 s/time step/cell on the IBM RS/6000 Model 530. This is approximately four times the CPU time for supersonic laminar flow and nine times that for the shock tube problem.

VI. Summary

The present work can be summarized as follows:

1) A numerical procedure for the full three-dimensional Navier–Stokes equations in which FVS and FDS are combined and the viscosity terms treated explicitly is presented in this paper. The procedure obviates the need for an explicit dissipation to control nonlinear stability. It also exploits the sharp shock resolution capability of approximate Riemman solvers as well as the relatively fast convergence of flux vector splitting methods. Very accurate calculations of laminar supersonic flows were observed, using the full Navier–Stokes equations. This conclusion is based on previous results[1,23–25] and the test problems in this paper.

2) In this work we have extended the foregoing approach to include the equations for the six components of the Reynolds stress and an additional equation for turbulence dissipation. Comparison of our turbulent calculations with recent experimental measurements of a Mach 2.87 supersonic turbulent boundary layer by Spina and Smits[6] show a reasonable agreement for the quantities compared. We also calculated a supersonic turbulent boundary layer experiencing the combined effects of an adverse pressure gradient, bulk compression, and concave streamline curvature.[26,27] The agreement with the experimental measurements was also very reasonable. The foregoing should establish the procedures presented in this paper as a viable one for supersonic turbulent flows.

Acknowledgments

This work was partially funded by NSF Grant CTS-9221630. The author will also like to express appreciation to D. L. Whitfield and Linda Kidd, both of Mississippi State University, for making available to him the extensive studies on this subject by Whitfield and his students. The useful discussions the author had with Robert Melnik of Northrop–Grumman are very much appreciated.

References

[1]Vanden, K. J., and Belk, D. M., "Numerical Investigation of Subsonic and Supersonic Axisymmetric Vortical Flows," *AIAA Journal*, Vol. 31, No. 8, 1993, pp. 1377–1383.

[2]Huang, P. G., and Coakley, T. J., "Turbulence Modeling for Complex Hypersonic Flows," AIAA Paper 93-0200, Jan. 1993.

[3]Baldwin, B. S., and Lomax, H., "Thin-Layer Approximation and Algebraic Model for Separated Turbulent Flows," AIAA Paper 78-257, Jan. 1978.

[4]Lee, J., Taulbee, D. B., and Holden, M. S., "Study of Turbulence on Supersonic Surfaces Using Reynolds Stress Model," *AIAA Journal*, Vol. 30, No. 7, 1992, pp. 739–746.

[5]Sarkar, S., and Lakshmanan, B., "Application of a Reynolds Stress Turbulence Model to the Compressible Shear Layer," *AIAA Journal*, Vol. 29, No. 5, 1991, pp. 743–749.

[6]Spina, E. F., and Smits, A. J., "Organized Structures in a Compressible, Turbulent Boundary Layer," *Journal of Fluid Mechanics*, Vol. 182, 1987, pp. 85–109.

[7]Wilcox, D. C., "Progress in Hypersonic Turbulent Modeling," AIAA Paper 91-1785, June 1991.

[8]Hortsman, C. C., "Prediction of Hypersonic Shock-Wave/Turbulent Boundary Layer Interaction Flows," AIAA Paper 87-1367, June 1987.

[9]Zeman, O., "On the Decay of Compressible Isotropic Turbulence," Center for Turbulence Research, CTR Manuscript 115, Stanford Univ., Stanford, CA, Aug. 1990.

[10]Zeman, O., and Blaisdell, G. A., "New Physics and Models for Compressible Turbulent Flows," *Advances in Turbulence*, Vol. 3, edited by A. V. Johanson and P. H. Alfredsson, Springer–Verlag, Berlin, pp. 445–454.

[11]Zeman, O., "A New Model for Super/Hypersonic Turbulent Boundary Layers," AIAA Paper 93-0897, Jan. 1993.

[12]Zeman, O., "Dilation Dissipation: The Concept and Application in Modeling, Compressible Mixing Layers," *Physics of Fluids*, Vol. A2, No. 2, 1990, pp. 178–188.

[13]Papamoschu, D., and Roshko, A., *Journal of Fluid Mechanics*, Vol. 197, 1988, p. 453.

[14]Roe, P. L., "The Use of the Riemann Problem in Finite-Difference Schemes," *Lecture Notes in Physics*, Vol. 141, 1980, pp. 354–359.

[15]Harten, A., and Lax, P. D., "A Random Choice Finite Difference Scheme for Hyperbolic Conservation Laws," *SIAM Journal of Numerical Analysis*, Vol. 18, 1981, pp. 289–315.

[16]Rusanov, V. V., *Zh. Vych. Matem. Mat. Fiz*, Vol. 1, No. 2, 1961, pp. 267–279.

[17]Van Leer, B., "Flux-Vector Splitting for the Euler Equations," *Eighth International Conference on Numerical Methods in Fluid Dynamics, Lecture Notes in Physics*, Vol. 170, 1982, pp. 507–512.

[18]Steger, J. L., and Warming, R. F., "Flux Vector Splitting of the Inviscid Gasdynamic Equations with Application to Finite-Difference Methods," *Journal of Computational Physics*, Vol. 40, 1981, pp. 263–293.

[19]Jameson, A., Schmidt, W., and Turkel, E., "Numerical Solutions of the Euler Equations by Finite Volume Methods Using Runge–Kutta Time-Stepping Schemes," AIAA Paper 81-1259, June 1991.

[20]MacCormack, R. W., "The Effect of Viscosity in Hypervelocity Impact Cratering," AIAA Paper 69-354, May 1969.

[21]Van Leer, B., Thomas, J. L., Roe, P. L., and Newsome, R. W., "A Comparison of Numerical Flux Formulas foir the Euler and Navier–Stokes Equation," AIAA Paper 87-1104-CP, June 1987.

[22]Quirk, J. J., "A Contribution to the Great Riemann Solver Debate," Institute of Computer Applications in Science and Engineering ICASE Rept. 92-64, 1992.

[23]Simpson, L. B., and Whitfield, D. L., "Flux-Difference Split Algorithm for Unsteady Thin-Layer Navier–Stokes Equations," *AIAA Journal*, Vol. 30, No. 4, 1992, pp. 914–922.

[24]Whitfield, D. L., "Implicit Upwind Finite Volume Scheme for the Three-Dimensional Euler Equations," Mississippi State Univ., Rept. MSSU-EIRS-ASE-85-1, Mississippi State, MS, Sept. 1985.

[25]Whitfield, D. L., "Implicit Finite Volume High Resolution Wave-Split Scheme," Mississippi State Univ. Rept. MSSU-EIRS-ASE-88-2, Mississippi State, MS, Feb. 1988.

[26]Jayaram, M., Taylor, M. W., and Smits, A., "The Response of a Compressible Turbulent Boundary Layer to Short Regions of Concave Surface Curvature," *Journal of Fluid Mechanics*, Vol. 175, 1987, pp. 343–362.

[27]Degani, D., and Smits, A. J., "Response of a Compressible, Turbulent Boundary Layer to a Short Region of Surface Curvature," *AIAA Journal*, Vol. 27, No. 1, 1989, pp. 23–28.

[28]Sarkar, S., Erlebacher, G., Hussaini, M. Y., and Kreiss, H. O., "The Analysis and Modeling of Dilational Terms in Compressible Turbulence," *Journal of Fluid Mechanics*, Vol. 227, 1991, pp. 473–493.

[29]Hanjalic, K., and Launder, B. E., "A Reynolds Stress Model of Turbulence and its Application to Thin Shear Flows," *Journal of Fluid Mechanics*, Vol. 52, 1972, pp. 609–638.

[30]Hanjalic, K., and Launder, B. E., "Contribution Towards a Reynolds-Stress Closure for Low-Reynolds-Number Turbulence," *Journal of Fluid Mechanics*, Vol. 74, 1976, pp. 593–610.

[31]Speziale, G., Sarkar, S., and Gatski, T. B., "Modelling the Pressure-Strain Correlation of Turbulence: An Invariant Dynamical Systems Approach," *Journal of Fluid Mechanics*, Vol. 227, 1991, pp. 245–272.

[32]Launder, B. E., Reece, G. J., and Rodi, W., "Progress in the Development of a Reynolds-Stress Turbulence Closure," *Journal of Fluid Mechanics*, Vol. 68, 1975, pp. 537–566.

[33]Launder, B. E., and Shima, N., "Second-Moment Closure for the Near-Wall Sublayer: Development and Applications," *AIAA Journal*, Vol. 27, No. 10, 1989, pp. 1319–1324.

[34]Lee, J., "Reynolds Stress Model Predictions of Supersonic Boundary Layer Over Compression Surfaces," Ph.D. Dissertation, State Univ. of New York, Buffalo, NY, Jan. 1991.

[35]Beam, R. M., and Warming, R. F., "An Implicit Finite Difference Algorithm for Hyperbolic Systems in Conservation Law Form," *Journal of Computational Physics*, Vol. 22, 1976, pp. 87–110.

[36]Gatlin, B., "An Implicit, Upwind Method for Obtaining Symbiotic Solutions to the Thin-Layer Navier–Stokes Equations," Ph.D. Dissertation, Mississippi State Univ., Mississippi State, MS, Aug. 1987.

[37]Roe, P. L., "Approximate Riemann Solvers, Parameter Vectors and Difference Schemes," *Journal of Computational Physics*, Vol. 43, 1981, pp. 263–293.

[38]Frink, N. T., "Upwind Scheme for Solving the Euler Equations on Unstructured Meshes," *AIAA Journal*, Vol. 30, No. 1, 1992, pp. 70–77.

[39]Sod, G. A., "A Survey of Several Finite Difference Methods for Systems of Nonlinear Hyperbolic Conservation Laws," *Journal of Computational Physics*, Vol. 27, 1978, pp. 1–31.

[40]Roe, P. L., "Characteristic-Based Schemes for the Euler Equations," *Annual Review of Fluid Mechanics*, Vol. 18, 1986, pp. 337–365.

[41]Shakib, F., "Finite-Element Analysis of the Compressible Euler and Navier–Stokes Equations," Ph.D. Dissertation, Stanford Univ., Stanford, CA, 1988.

[42]Fernholtz, H. H., Finley, P. J., Dussauge, J. P., and Smits, A. J., "A Survey of Measurements and Measuring Techniques in Rapidly Distorted Compressible Turbulent Boundary Layers," AGARD 315, 1989.

[43]Gerolymos, G. A., "Implicit Multi-Grid Solution of the Compressible Navier–Stokes Equations Using k–ϵ Turbulence Closure," *AIAA Journal*, Vol. 28, No. 10, 1990, pp. 1707–1717.

[44]Demuren, A. O., and Sarkar, S., "Systematic Study of Reynolds Stress Closure Models in the Computations of Plane Channel Flows," Institute for Computer Applications in Science and Engineering, ICASE Rept. 92-19, 1992.

[45]Van Driest, E. R., "Turbulent Boundary Layer in Compressible Fluids," *Journal of Aeronautical Science*, Vol. 18, 1951, pp. 145–160.

[46]Grasso, F., and Falconi, D., "High-Speed Turbulence Modeling of Shock-Wave/Boundary Layer Interaction," *AIAA Journal*, Vol. 31, No. 7, 1993, pp. 1199–1206.